Molecular Cancer Therapeutics

A Patient-derived Xenograft Model of Pancreatic Neuroendocrine Tumors Identifies Sapanisertib as a Possible New Treatment for Everolimus-resistant Tumors

Chester E. Chamberlain[1,2,3], Michael S. German[1,2,3], Katherine Yang[1,2,3], Jason Wang[1,2,3], Henry VanBrocklin[4], Melanie Regan[4], Kevan M. Shokat[5], Gregory S. Ducker[5], Grace E. Kim[6], Byron Hann[7], David B. Donner[7,8], Robert S. Warren[7,8], Alan P. Venook[3,7], Emily K. Bergsland[3,7], Danny Lee[7,8], Yucheng Wang[7,8], and Eric K. Nakakura[7,8]

Abstract

Patients with pancreatic neuroendocrine tumors (PNET) commonly develop advanced disease and require systemic therapy. However, treatment options remain limited, in part, because experimental models that reliably emulate PNET disease are lacking. We therefore developed a patient-derived xenograft model of PNET (PDX-PNET), which we then used to evaluate two mTOR inhibitor drugs: FDA-approved everolimus and the investigational new drug sapanisertib. PDX-PNETs maintained a PNET morphology and PNET-specific gene expression signature with serial passage. PDX-PNETs also harbored mutations in genes previously associated with PNETs (such as *MEN1* and *PTEN*), displayed activation of the mTOR pathway, and could be detected by Gallium-68 DOTATATE PET-CT. Treatment of PDX-PNETs with either everolimus or sapanisertib strongly inhibited growth. As seen in patients, some PDX-PNETs developed resistance to everolimus. However, sapanisertib, a more potent inhibitor of the mTOR pathway, caused tumor shrinkage in most everolimus-resistant tumors. Our PDX-PNET model is the first available, validated PDX model for PNET, and preclinical data from the use of this model suggest that sapanisertib may be an effective new treatment option for patients with PNET or everolimus-resistant PNET.
Mol Cancer Ther; 17(12); 2702–9. ©2018 AACR.

Introduction

Pancreatic neuroendocrine tumors (PNET) are a form of pancreatic neoplasm with neuroendocrine features whose precise cell of origin is unknown. PNETs comprise approximately 10% of all pancreatic malignancies (1), can cause diverse clinical syndromes (2), and have a 5-year mortality rate of approximately 60% (1, 3). PNETs can be either sporadic or the consequence of a hereditary cancer syndrome, such as multiple endocrine neoplasia type 1 (MEN1). Two-thirds of patients diagnosed with PNET have unresectable metastatic disease and therefore require systemic therapy.

Activated mTOR signaling is present in about 14% of PNETs and is associated with a poor prognosis (4). mTOR is a serine-threonine kinase that serves as the catalytic subunit of two distinct signaling complexes, mTORC1 and mTORC2. mTORC1 promotes cell growth through two key effectors: p70S6 Kinase 1 (S6K1) and eIF4E-binding protein 1 (4EBP1). mTORC1 directly phosphorylates S6K1, which can then phosphorylate several downstream substrates such as ribosomal protein S6 (RPS6). 4EBP1 is inactivated by mTORC1 phosphorylation, initiating the translation of proteins. mTORC2 promotes cell proliferation and survival through activation of AKT by phosphorylation (5).

Activation of the mTOR pathway in PNETs results from mutations in genes that encode negative regulators of the pathway, such as *PTEN* (4, 6, 7). The best known mTOR inhibitor drug is rapamycin, which forms a complex with 12-kDa FK506-binding protein (FKBP12) to inhibit mTORC1. Because of mTOR's central importance in many human diseases, there are many efforts to develop drugs that more effectively inhibit its activity (8). The mTOR inhibitor drug everolimus, a derivative of rapamycin (8), has been approved by the FDA for the treatment of advanced PNETs and other tumors (9, 10). Everolimus, like rapamycin and other homologous agents (rapalogs), allosterically inhibits mTORC1 but does not affect mTORC2. It can also fail to block the phosphorylation of mTORC1 target 4EBP1, and paradoxically increase the activation of AKT due to suppression of a negative feedback loop (11). Clinically, everolimus typically delays human PNET progression by several months, but significant tumor shrinkage is unlikely and eventual resistance is the rule. Sapanisertib (INK128), is a second-generation mTOR inhibitor drug that

[1]Center for Regeneration Medicine, University of California, San Francisco, California. [2]Diabetes Center, University of California, San Francisco, California. [3]Department of Medicine, University of California, San Francisco, California. [4]Department of Radiology and Biomedical Imaging, University of California, San Francisco, California. [5]Department of Cellular Molecular Pharmacology, University of California, San Francisco, California. [6]Department of Pathology, University of California, San Francisco, California. [7]Helen Diller Family HDF Comprehensive Cancer Center, University of California, San Francisco, California. [8]Department of Surgery, University of California, San Francisco, California.

Note: Supplementary data for this article are available at Molecular Cancer Therapeutics Online (http://mct.aacrjournals.org/).

Corresponding Authors: Eric K. Nakakura, University of California, 1600 Divisadero Street, A-724, San Francisco, CA 94143-1932. Phone: 415-353-9294; Fax: 415-353-9695; E-mail: eric.nakakura@ucsf.edu; Chester E. Chamberlain, chester.chamberlain@ucsf.edu

doi: 10.1158/1535-7163.MCT-17-1204

directly binds to the ATP-binding site of mTOR, thereby potently inhibiting both mTORC1 and mTORC2 (12), and overcoming the everolimus-resistant phosphorylation of 4EBP1 and AKT (13, 14). Also in contrast to rapalogs, sapanisertib has strong cytotoxic activity toward tumors (15–17).

Patient-derived xenografts (PDX) have emerged as an important platform to elucidate new treatments and biomarkers for cancer (18–21). Human tumor samples, typically derived from biopsy or surgical samples, are implanted and propagated in nude mice in an effort to generate PDX lines that retain signaling pathways (22) and the idiosyncratic intratumor heterogeneity that typifies human cancer (23–25). PDX models have proven to be particularly useful tools for predicting the effectiveness of new drug therapies (26–29), and modeling drug resistance (30, 31). Although multiple PDX models have been successfully developed for pancreatic ductal adenocarcinoma (32, 33) and other cancers (20, 21), a PDX model for PNETs has not been described.

Here we report the establishment of the first PDX model for PNETs, and show using this model that the second-generation mTOR inhibitor drug sapanisertib may serve as an effective new treatment option for patients with PNET and everolimus-resistant PNET.

Materials and Methods

PNET xenografts

Patient written informed consent was obtained, and the research protocol was approved by the Institutional Review Board of the University of California, San Francisco. All animal studies were conducted under an animal use protocol approved by the University of California San Francisco Animal Care and Use Committee. A patient with an advanced PNET producing insulin underwent palliative debulking of liver metastases to ameliorate symptomatic hypoglycemia. To establish xenografts, nondiagnostic portions of tumors removed during the hepatic resection were minced under aseptic conditions and approximately 20 μL of tumor:Matrigel (1:1) implanted subcutaneously into female athymic nude mice (Envigo). Nonimplanted fragments were flash-frozen in liquid nitrogen and banked. For the initial implantation, bilateral injections were made into the flanks of mice to establish the xenograft passage 0 (P0). When tumor burden reached approximately 700 to 1,000 mm^3, mice were sacrificed; tumors were then resected, processed, and injected subcutaneously into new recipient animals. To establish cohorts of mice for drug trials, individual tumors were implanted into 4 to 5 mice and allowed to reach maximum protocol size. Tumors were then minced and implanted into 30 mice and allowed to grow. When the average tumor size of the cohort reached 150 mm^3, animals with high and low tumor volumes were discarded from the study and the remaining animals randomized into control and treatment groups on the basis of tumor volume. Tumor volume was measured every 3 to 7 days during drug treatment. For single-arm drug studies, waterfall plots were used to summarize the distribution of tumor growth responses to treatments, as described previously (34). Briefly, the tumor size at the start of treatment was defined as the baseline volume, and the smallest tumor volume recorded during treatment was defined as the best response. If the tumor did not respond and its size did not decrease below baseline throughout treatment, then the largest change in tumor size up to 100% was used instead.

Drug treatment

Everolimus was purchased commercially and sapanisertib was synthesized by K.M. Shokat and G.S. Ducker. The drugs were prepared as 2.5 mg/mL suspensions in a vehicle of 5% 1-methyl-2 pyrrolidinone (NMP), 80% polyvinyl pyrralidone (PVP), and 15% water for initial pharmacodynamic studies, and then in 3.1% NMP, 81.6% PVP, 15.3% water for tumor regression studies to reduce toxicity. Single tumor-bearing mice were dosed once daily with 10 mg/kg body weight (BW) everolimus, 1 mg/kg BW sapanisertib, or vehicle by oral gavage (OG). Mice were sacrificed, and tumors harvested and split and paraffin embedded for histologic analysis or flash frozen for whole tissue Western blotting analysis and molecular interrogation at experimental endpoints.

MicroPET Imaging

^{68}Ga-DOTATATE was prepared and purified in the UCSF radiochemistry laboratory. Briefly, $^{68}GaCl_3$ was eluted from a ^{68}Ge/^{68}Ga generator (Eckert & Ziegler) and reacted with DOTATATE (DOTA0, Tyr3, Thr8]octreotide) in sodium acetate buffer. Solid-phase extraction purification gave ^{68}Ga-DOTATATE in injectable ethanol/saline solution. PNET-PDX mice were injected with 120–180 μCi (4.4–6.7 MBq) of ^{68}Ga-DOTATATE through a tail vein catheter. Static PET/CT images were taken on a Siemens Inveon microPET/CT scanner for 30 minutes at 2.75 hours post tracer injection. Images were reconstructed and viewed using AMIDE software (freeware, amide.sourceforge.net).

Western blot analysis

All antibodies for Western blot analysis were purchased from Cell Signaling Technology. Blots were visualized by using either horseradish peroxidase (HRP)-conjugated secondary antibodies and chemiluminescent reagent from Pierce Protein Research Products or by fluorescent secondary antibodies. GAPDH was used as an internal control and each experiment was done in independent biological duplicates.

IHC

Tissues were fixed in Z-fix (Anatech) and processed for paraffin or frozen sections using standard methods. The following primary antibodies were used: rabbit anti-CHGA (Immunostar); rabbit anti-5-HT (Immunostar); mouse monoclonal anti-5-HT (Dako), guinea pig polyclonal anti-INS (Dako), mouse monoclonal anti-Ki-67 (clone MIB-1, Dako). Secondary antibodies (Jackson ImmunoResearch) were FITC-conjugated goat anti-mouse and anti-rabbit; FITC-conjugated donkey anti-goat and anti-mouse; Cy3-conjugated donkey anti-goat, goat anti-mouse, and anti-rabbit; HRP-conjugated goat anti-mouse and anti-rabbit. Slides were imaged on an Axioskop 2 microscope (Zeiss) or on an LSM510 META confocal microscope (Zeiss). Ki-67 was used to assess proliferation. The mitotic index was calculated on the hematoxylin and eosin sections for the histology samples according to the 2010 WHO guidelines. Ki-67 indices for the cell block sections were calculated as the total number of tumor cells with positive nuclear staining divided by the total number of tumor cells present.

Whole-exome sequencing

Genomic DNA was extracted using standard procedures. Targeted capture and massive parallel sequencing were performed at the UCSF Institute for Human Genetics (San

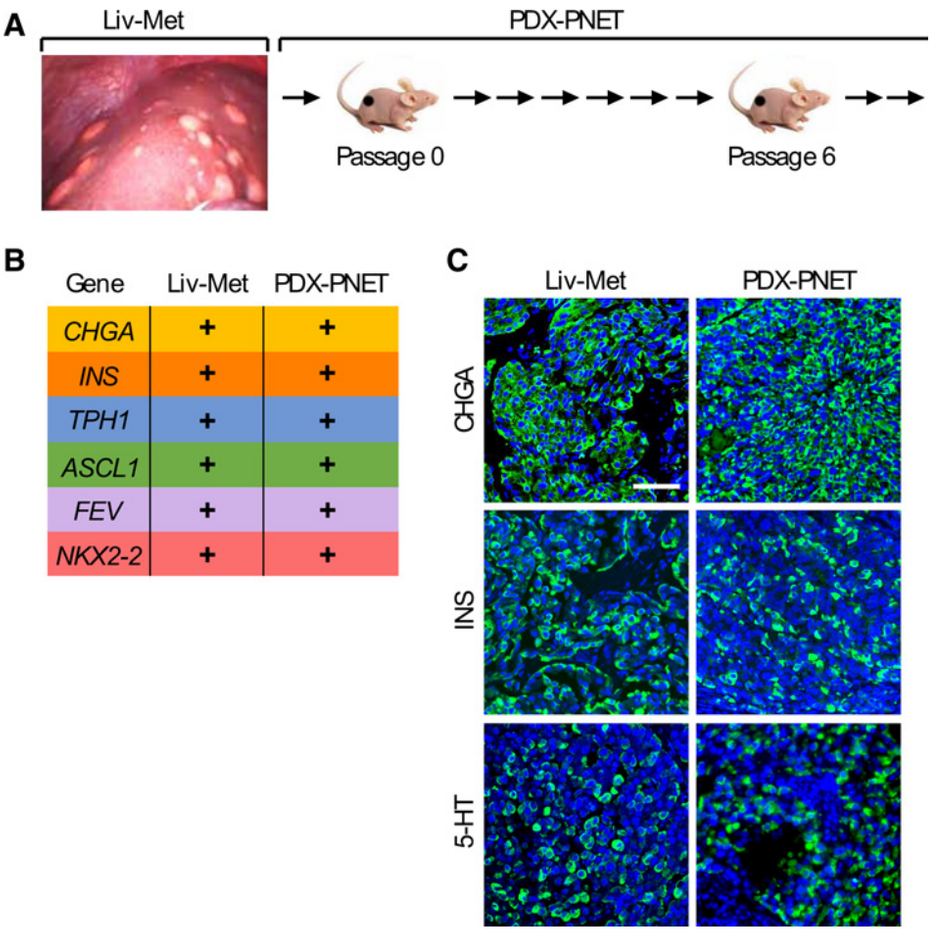

Figure 1.
Generation and characterization of the patient-derived xenograft model of PNET (PDX-PNET). **A,** nondiagnostic portion of metastasized PNETs were removed during the hepatic resection and expanded in a cohort of female athymic nude mice. Comparison of neuroendocrine biomarkers in original patient tumor and passage-6 PDX-PNET using RNA sequencing (**B**) and immunofluorescence (**C**). In **B,** a "+" means a gene is expressed. In **C,** DNA is in blue while CHGA, INS, and 5-HT are in green.

Francisco, CA). Briefly, genomic DNA was sheared by Covaris S2 to a target size of 200 to 300 bp and assembled into a library with TruSeq adapters containing indexes that differentiate different libraries in a capture reaction as well as a sequencing run (Kapa Biosystems). Libraries were pooled into a capture reaction that contains biotinylated DNA oligonucleotides (called "baits") from Roche-Nimblegen SeqCap EZ Human Exome Library v3.0 for 72 hours. The DNA bait-DNA hybrids were then pulled out of the complex mixture by incubation with streptavidin-labeled magnetic beads and captured onto a strong magnet. After washing, the targeted DNA of interest was eluted and subjected to 18 cycles of DNA amplification. Captured DNA libraries were sequenced with the Illumina HiSeq 2500, yielding 150 (2×75) base pairs from the final library fragments. Sequence data were mapped to the GRCh37 reference genome and processed using the Bina Genomic Analysis Platform. Somatic mutation caller tools included JointSNVMix (35), MuTect (35), Somatic Sniper (36), VarDict (37), and VarScan (37). Somatic mutations were also filtered on the basis of read quality, allele frequency [dbSNP (38), 1000 Genomes (39), ExAC (40), COSMIC (41)], and functional effect [SIFT (42), Polyphen (43), SnpEff (44)]. Sequencing data can be found at the Sequence Read Archive (SRA Study accession number: SRP162135).

Results

Development and characterization of a PDX model of PNET

To establish xenografts, nondiagnostic portions of PNET liver metastasis tissue were removed during partial hepatic resection surgery in a patient with an advanced, well-differentiated PNET producing insulin, processed as described and subcutaneously implanted into female athymic nude mice (Fig. 1A). The successfully engrafted tumor maintained the characteristics of the patient tumor tissue through multiple rounds of serial transplantation in athymic mice to successfully establish this PDX-PNET.

We compared gene expression between the original patient PNET liver metastasis tissue (Liv-Met) and PDX-PNET tissue harvested at passage 6 (Fig. 1B). Using RNA sequencing (RNA-seq), we detected the expression of neuroendocrine tumor genes *CHGA*, *INS*, and *TPH1* (2). We also detected *NKX2-2*, *ASCL1*, and *FEV*, which encode developmental transcription factors critical to the differentiation and hormone expression of neuroendocrine tumors (45, 46). Consistent with this, immunofluorescence analysis of tissue sections revealed strong expression of CHGA, INS, and 5-HT, the metabolic product of TPH1, in both Liv-Met and PDX-PNET tissues (Fig. 1C). PDX-PNETs also retained a well-differentiated neuroendocrine tumor morphology with a Ki-67 index of 6% to 8% (G2).

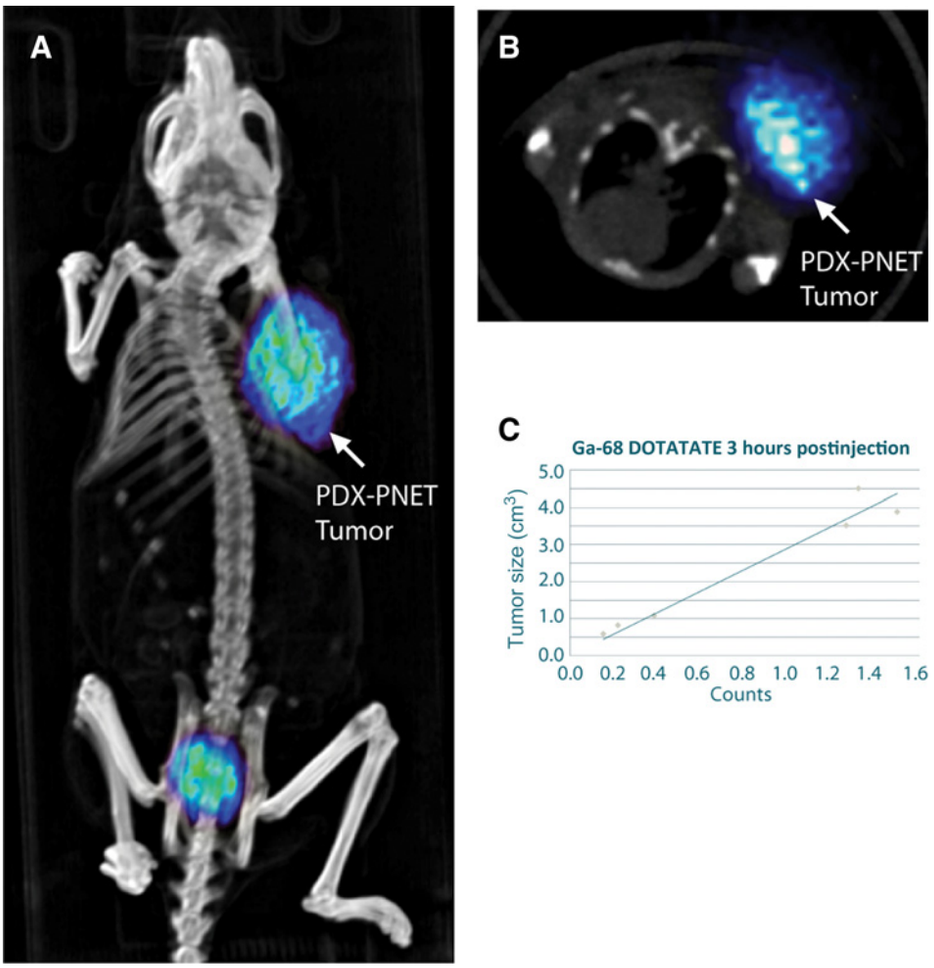

Figure 2.
^{68}Ga-DOTATATE PET-CT imaging of the PDX-PNET model. **A,** 3D rendered PET/CT image showing flank tumor tracer uptake. **B,** Axial view at the level of the tumor. **C,** Relationship between tumor size and normalized ^{68}Ga-DOTATATE PET/CT counts.

PNETs express somatostatin receptors (47); consequently, the radiolabeled somatostatin analogue Gallium-68 DOTATATE is used as a tracer for positron emission tomography–computed tomography (PET-CT) imaging of PNETs in the clinic (48). We therefore evaluated whether Gallium-68 DOTATATE could be used to perform functional PET-CT imaging of PDX-PNETs *in vivo*. At 3 hours postinjection, Gallium-68 DOTATATE PET-CT clearly colocalized with the subcutaneous PDX-PNETs (Fig. 2), showing that Gallium-68 DOTATATE can be used to perform functional PET-CT imaging in this model. Importantly, a linear relationship was observed between tumor volume and normalized Gallium-68 DOTATATE counts over a large range of tumor size (Fig. 2C).

Using whole-exome sequencing to identify genetic mutations harbored in the PDX-PNET model, we found that PDX-PNETs contained mutations in known PNET-associated genes (4, 6), such as *MEN1*, *BRCA2*, *PTEN*, and *SETD2* (Fig. 3A). We did not observe mutations in genes commonly associated with pancreatic ductal adenocarcinoma, such as *KRAS*, *TP53*, *CDKN2A*, *SMAD3*, *SMAD4*, and *TGFBR1* (49, 50). Together, these findings provide strong evidence that the PDX-PNET model is a bona fide PNET model.

Evaluating mTOR inhibitor drugs everolimus and sapanisertib in the PDX-PNET model

PTEN functions as an inhibitor of the mTOR pathway (51). Mutations in *PTEN* cause mTOR pathway activation (51), and can predict tumor response to mTOR inhibitor drugs (52). We found two deleterious frameshift mutations in *PTEN* (Fig. 3B), suggesting mTOR pathway activation in the PDX-PNET model. Consistent with this, Western blot analysis revealed phosphorylation of the mTORC1 downstream targets 4EBP1 and RPS6 (Fig. 4B; lanes 1–3). We also detected the phosphorylation of mTORC2 target AKT. Phosphorylation of S6K1, a substrate of mTORC1 that phosphorylates RPS6, was barely detectable in PDX-PNETs.

Everolimus, an mTOR inhibitor drug that inhibits mTORC1 but not mTORC2, demonstrated unequivocal antitumor activity in a phase III study leading to its approval for the treatment of advanced PNETs (9). We therefore evaluated the response of PDX-PNETs to treatment with everolimus. We also evaluated sapanisertib, a second-generation mTOR inhibitor that directly binds the ATP-binding site of mTOR and inhibits both mTORC1 and mTORC2 (12). The optimal everolimus and sapanisertib dose was determined by pharmacodynamic studies (Supplementary Fig. S1). Single tumor-bearing mice were treated once daily with everolimus (10 mg/kg BW), sapanisertib (1 mg/kg BW), or vehicle by oral gavage for 28 days. Treatment was well tolerated in all groups. We found that vehicle-treated control PDX-PNETs grew several fold in size ($n = 5$; Fig. 4A). In contrast, the growth of PDX-PNETs treated with either everolimus ($n = 6$) or sapanisertib ($n = 6$) was significantly blocked (Fig. 4A).

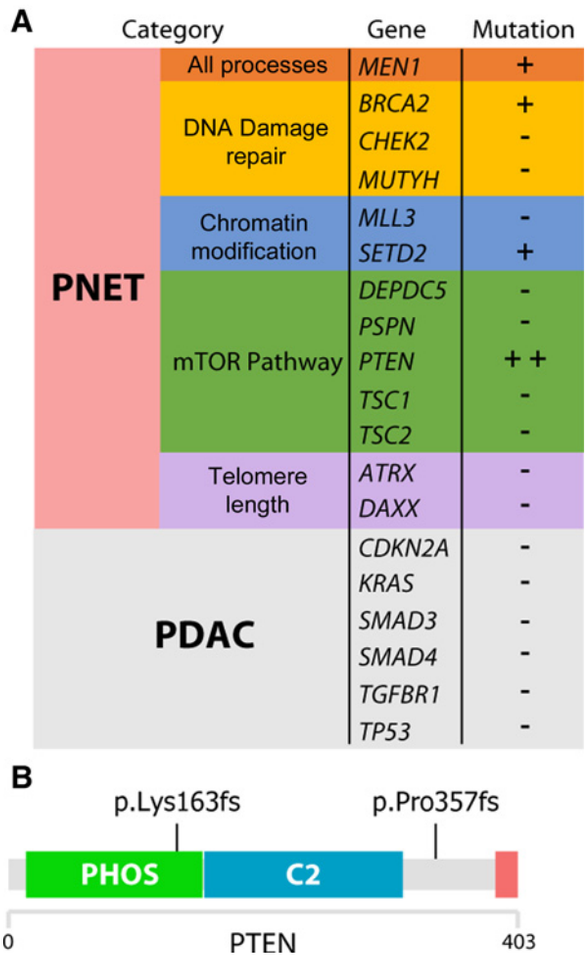

Figure 3.

PDX-PNETs harbor mutations in genes commonly associated with PNETs and mTOR pathway activation. **A,** Whole-exome sequencing of PDX-PNET reveals mutations in genes commonly found in PNET. **B,** Two frameshift mutations were identified in *PTEN*. Green, phosphatase domain; blue, C2 domain; red, PDZ-binding domain.

To evaluate the *in vivo* effects of everolimus and sapanisertib on mTOR pathway targets, we harvested PDX-PNET tissues and performed Western blot analysis. Everolimus completely inhibited the phosphorylation of mTORC1 target RPS6, but not 4EBP1 (Fig. 4B; lanes 4–6). AKT phosphorylation was increased, consistent with rapalogs having no activity toward mTORC2 targets and the feedback activation of AKT that has been observed in human trials with other rapamycin derivatives (11). In contrast, sapanisertib inhibited the phosphorylation of both mTORC1 targets 4EBP1 and RPS6 (Fig. 4B; lanes 7–9). Also in contrast to everolimus, sapanisertib inhibited the phosphorylation of the mTORC2 target AKT. These findings demonstrate that sapanisertib more completely inhibits the mTOR pathway than everolimus in the PDX-PNETs.

The PDX-PNET model for studying acquired drug resistance in PNETs

The development of drug resistance is a major limitation of PNET clinical response to everolimus treatment (53). We therefore sought to generate everolimus-resistant PDX-PNETs by treating a large cohort of tumor-bearing animals once daily with everolimus for several months ($n = 34$). Because this was a single-arm study, everolimus resistance was defined as a doubling in the tumor volume from the day of treatment. The baseline volume was defined as the tumor size at the start of treatment, and the smallest tumor volume recorded during treatment was defined as the best response (34). If the tumor failed to respond, then the largest change in tumor size up to 100% was used for the best response. In Fig. 5A, animals are listed in order of increasing percentage response to everolimus. Most PDX-PNETs (29/34) experienced a reduction in tumor volume during everolimus treatment (Fig. 5A; numbers 6–34), five failed to respond (Fig. 5A; numbers 1–5), and seven experienced complete regression (Fig. 5A; numbers 28–34). The variability in response may be because of the heterogeneous nature of the PDX-PNET model (23–25) or experimental variation. From this group, 10 everolimus-resistant PDX-PNETs were identified (Fig. 5B). Although all 10 everolimus-resistant tumors doubled in size during everolimus treatment, their time to resistance was variable, ranging between 7 and 236 days, and with a median time to resistance of 110 days. The best response of the 10 everolimus-resistant PDX-PNETs to everolimus was also variable, with some not responding at all (Fig. 5A; numbers 1 and 3), and others responding with a greater than 50% reduction in tumor volume (Fig. 5A; numbers 22 and 23).

Everolimus partially inhibits mTORC1 and fails to inhibit mTORC2, suggesting that resistance to everolimus may be overcome by the more potent mTOR pathway inhibitor drug sapanisertib, which inhibits both mTORC1 and mTORC2. We therefore

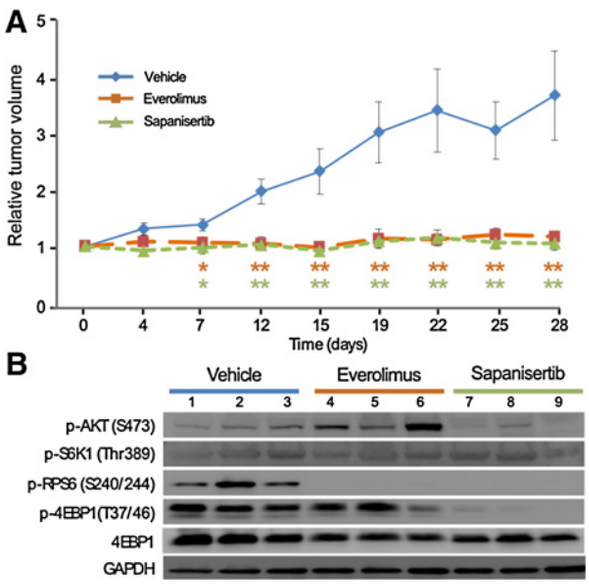

Figure 4.

Response of PDX-PNETs to the mTOR inhibitor drugs everolimus and sapanisertib. **A,** Growth chart of PDX-PNETs treated with vehicle control, everolimus, or sapanisertib for 28 days (vehicle control $n = 5$, everolimus $n = 6$, sapanisertib $n = 6$). The P values were calculated by two-tailed Student t test (*, $P < 0.05$, **, $P < 0.01$). Error bars indicate the SD from the mean. **B,** Western blot analysis of mTOR pathway targets in PDX-PNETs harvested after 28 days of treatment with either vehicle control, everolimus, or sapanisertib. Each lane represents a single xenograft harvested from a unique mouse.

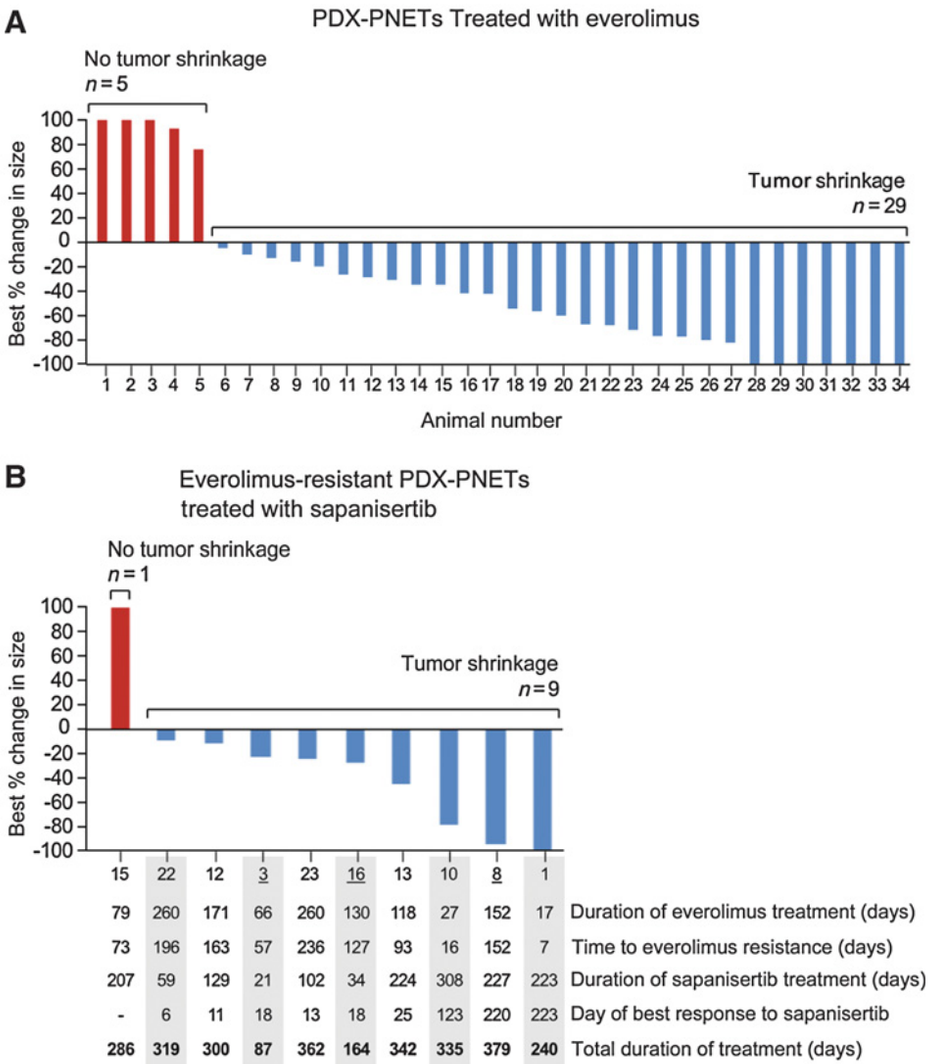

Figure 5.
Response of everolimus-resistant PDX-PNETs to sapanisertib. **A,** The best response of tumors treated with everolimus, as compared with pretreatment baseline ($n = 34$). Numbers along the *x*-axis indicate arbitrarily assigned animal numbers in order of increasing percentage response to everolimus. The bars indicate the percent change in tumor burden from baseline. **B,** The best response to sapanisertib in 10 animals with everolimus-resistant PDX-PNETs. Selected tumor characteristics are listed in the table below the graph. Animals are listed in order of increasing percentage response to sapanisertib, with listed numbers corresponding to those in Fig. 5A. Sapanisertib treatment ended when tumors either regressed ($n = 1$), developed sapanisertib resistance, and exceeded five times the original volume ($n = 6$), or animals died ($n = 3$). Underlined numbers indicate animals that died during treatment.

evaluated the effect of sapanisertib treatment on everolimus-resistant PDX-PNETs (Fig. 5B). In Fig. 5B, animals are listed in order of increasing percentage response to sapanisertib, with listed numbers corresponding to those in Fig. 5A. We found that most everolimus-resistant PDX-PNETs (9/10) experienced a reduction in tumor volume during sapanisertib treatment, one failed to respond, and one experienced complete regression. The everolimus-resistant PDX-PNET that completely regressed during sapanisertib treatment had not responded to everolimus treatment (Fig. 5; number 1), whereas the everolimus-resistant PDX-PNET that did not respond to sapanisertib had a moderate response to everolimus (Fig. 5; number 15).

Discussion

Patient-derived xenograft (PDX) models have proven to be extremely useful in drug discovery research (18–21). Unlike cell lines and many genetically engineered mouse models, PDX models retain the cellular and genetic heterogeneity of the primary human tumor (23–25) and may therefore better model many important aspects of the disease, such as drug resistance (30, 31). We report the establishment of the first PDX model for PDX-PNETs. We also refer to this as the HNV PDX-PNET model as the implanted tumor tissue had been resected from segment V of the patient's liver. There have been many previous attempts by us and other groups to establish a PDX model of PNET. We do not know why this one was successful, but the PNET was unusually aggressive, had metastasized, and ultimately killed the patient. We speculate that the unique aggressiveness of the tumor enabled it to successfully survive and grow in a foreign mouse host. Identifying a molecular cause for this aggressiveness is not trivial, especially as this is currently an n of 1. Additional sequencing analyses and the establishment of additional PDX-PNET models may provide some insight.

Histologic analysis, gene expression profiling, and whole-exome sequencing confirmed that the PDX-PNETs retained the hallmark features of PNETs. Interestingly, PDX-PNETs harbored *PTEN* mutations and responded to mTOR inhibitor drugs everolimus and sapanisertib, suggesting that the PNET mutational profile may determine drug response. In addition to *PTEN*,

PDX-PNETs harbored mutations in *MEN1* and *BRCA2* (Fig. 3). *MEN1* encodes the tumor-suppressive menin and germline mutations in *MEN1* cause multiple endocrine neoplasia type 1 (MEN1; ref. 54). A recent study identified a synthetic lethal interaction between *MEN1* mutation and MEK1/2 inhibition in neuroendocrine cells (55), suggesting that MEK1/2 inhibitor drugs FDA-approved for other cancers such as trametinib or cobimetinib may have clinical activity against PNETs. Loss of *BRCA2* drives one of the mutational signatures found in PNETs (4, 56) and PARP inhibitors have shown promise in clinical studies against *BRCA2*-mutated tumors (57, 58). Future studies evaluating these treatments on PDX-PNETs may be informative.

PDX-PNETs responded equally to everolimus and sapanisertib despite everolimus treatment leading to AKT activation and not suppressing p4EBP (Fig. 4), suggesting that these are not the mechanisms of resistance, at least in the short term. Comparing time to progression may reveal a potential benefit for sapanisertib over everolimus, and would also more closely resemble endpoints used in clinical trials. One particularly promising finding from our study was that the majority of everolimus-resistant PDX-PNETs responded to sapanisertib (Fig. 5), which directly targets mTOR and inhibits the activity of both mTORC1 and mTORC2 (8). Sapanisertib is currently being evaluated in multiple cancers across 11 clinical trials, including a phase II study of rapalog-resistant advanced PNET (ClinicalTrials.gov Identifier: NCT02893930). The results from this trial may help clarify the value of the HNV PDX-PNET model in selecting PNET therapies and identifying PNET biomarkers of drug response and resistance.

Disclosure of Potential Conflicts of Interest

K. Shokat is a consultant/advisory board member for Takeda Pharmaceuticals and has ownership interest including stocks and patents in Takeda Pharmaceuticals. E.K. Bergsland has received speakers bureau honoraria from UpToDate. No potential conflicts of interest were disclosed by the other authors.

Authors' Contributions

Conception and design: C.E. Chamberlain, M.S. German, Y. Wang, E.K. Nakakura

Development of methodology: C.E. Chamberlain, H. VanBrocklin, G.S. Ducker, B.Hann, D.B. Donner, Y. Wang, E.K. Nakakura

Acquisition of data (provided animals, acquired and managed patients, provided facilities, etc.): C.E. Chamberlain, K. Yang, H. VanBrocklin, K.M. Shokat, B.Hann, A.P. Venook, D. Lee, Y. Wang, E.K. Nakakura

Analysis and interpretation of data (e.g., statistical analysis, biostatistics, computational analysis): C.E. Chamberlain, M.S. German, J.Wang, R.S. Warren, D. Lee, Y. Wang, E.K. Nakakura

Writing, review, and/or revision of the manuscript: C.E. Chamberlain, M.S. German, H. VanBrocklin, D.B. Donner, R.S. Warren, A.P. Venook, E.K. Bergsland, E.K. Nakakura

Administrative, technical, or material support (i.e., reporting or organizing data, constructing databases): M. Regan, D. Lee, E.K. Nakakura

Study supervision: C.E. Chamberlain, M.S. German, E.K. Nakakura

Others (reviewed the pathology and interpreted the stain results): G.E. Kim

Other (provided the sapanisertib for the study): K.M. Shokat

Acknowledgments

The authors would like to thank Bina and Roche for use of their genomic bioinformatic platform and expert advice, the UCSF Preclinical Therapeutics Core for their help with HNV PDX-PNET model development and preclinical study execution, Pamela Derish for expert help with writing and preparation of the manuscript, the Placzek Family Foundation for their generous support, and Larry and Margaret Hauben for their vision and unwavering support. This work was supported by grants from the Neuroendocrine Tumor Research Foundation (NETRF; to E.K. Nakakura, C.E. Chamberlain, and M.S. German), the NIH (P30 DK63720, to M.S. German), and the NETRF-American Association for Cancer Research Grant (AACR grant no. 12-60-33-NAKA, to E. K. Nakakura).

The costs of publication of this article were defrayed in part by the payment of page charges. This article must therefore be hereby marked *advertisement* in accordance with 18 U.S.C. Section 1734 solely to indicate this fact.

Received December 3, 2017; revised July 18, 2018; accepted September 20, 2018; published first September 25, 2018.

References

1. Yao JC, Eisner MP, Leary C, Dagohoy C, Phan A, Rashid A, et al. Population-based study of islet cell carcinoma. Ann Surg Oncol 2007;14:3492–500.
2. Yao JC, Hassan M, Phan A, Dagohoy C, Leary C, Mares JE, et al. One hundred years after "carcinoid": epidemiology of and prognostic factors for neuroendocrine tumors in 35,825 cases in the United States. J Clin Oncol 2008;26:3063–72.
3. Bosman FT, Carneiro F, Hruban RH, Theise ND. WHO classification of tumours of the digestive system. Lyon, France: International Agency for Research on Cancer; 2010.
4. Scarpa A, Chang DK, Nones K, Corbo V, Patch AM, Bailey P, et al. Whole-genome landscape of pancreatic neuroendocrine tumours. Nature 2017; 543:65–71.
5. Saxton RA, Sabatini DM. mTOR signaling in growth, metabolism, and disease. Cell 2017;168:960–76.
6. Jiao Y, Shi C, Edil BH, de Wilde RF, Klimstra DS, Maitra A, et al. DAXX/ATRX, MEN1, and mTOR pathway genes are frequently altered in pancreatic neuroendocrine tumors. Science 2011;331:1199–203.
7. Missiaglia E, Dalai I, Barbi S, Beghelli S, Falconi M, della Peruta M, et al. Pancreatic endocrine tumors: expression profiling evidences a role for AKT-mTOR pathway. J Clin Oncol 2010;28:245–55.
8. Benjamin D, Colombi M, Moroni C, Hall MN. Rapamycin passes the torch: a new generation of mTOR inhibitors. Nat Rev Drug Discov 2011; 10:868–80.
9. Yao JC, Shah MH, Ito T, Bohas CL, Wolin EM, Van Cutsem E, et al. Everolimus for advanced pancreatic neuroendocrine tumors. N Engl J Med 2011;364:514–23.
10. Yao JC, Fazio N, Singh S, Buzzoni R, Carnaghi C, Wolin E, et al. Everolimus for the treatment of advanced, non-functional neuroendocrine tumours of the lung or gastrointestinal tract (RADIANT-4): a randomised, placebo-controlled, phase 3 study. Lancet 2016;387:968–77.
11. O'Reilly KE, Rojo F, She QB, Solit D, Mills GB, Smith D, et al. mTOR inhibition induces upstream receptor tyrosine kinase signaling and activates Akt. Cancer Res 2006;66:1500–8.
12. Hsieh AC, Liu Y, Edlind MP, Ingolia NT, Janes MR, Sher A, et al. The translational landscape of mTOR signalling steers cancer initiation and metastasis. Nature 2012;485:55–61.
13. Feldman ME, Apsel B, Uotila A, Loewith R, Knight ZA, Ruggero D, et al. Active-site inhibitors of mTOR target rapamycin-resistant outputs of mTORC1 and mTORC2. PLoS Biol 2009;7:e38.
14. Thoreen CC, Kang SA, Chang JW, Liu Q, Zhang J, Gao Y, et al. An ATP-competitive mammalian target of rapamycin inhibitor reveals rapamycin-resistant functions of mTORC1. J Biol Chem 2009;284: 8023–32.
15. Hsieh AC, Costa M, Zollo O, Davis C, Feldman ME, Testa JR, et al. Genetic dissection of the oncogenic mTOR pathway reveals druggable addiction to translational control via 4EBP-eIF4E. Cancer Cell 2010;17:249–61.
16. Janes MR, Limon JJ, So L, Chen J, Lim RJ, Chavez MA, et al. Effective and selective targeting of leukemia cells using a TORC1/2 kinase inhibitor. Nat Med 2010;16:205–13.
17. Hsieh AC, Ruggero D. Targeting eukaryotic translation initiation factor 4E (eIF4E) in cancer. Clin Cancer Res 2010;16:4914–20.
18. Hidalgo M, Amant F, Biankin AV, Budinska E, Byrne AT, Caldas C, et al. Patient-derived xenograft models: an emerging platform for translational cancer research. Cancer Discov 2014;4:998–1013.
19. Siolas D, Hannon GJ. Patient-derived tumor xenografts: transforming clinical samples into mouse models. Cancer Res 2013;73:5315–9.

20. Tentler JJ, Tan AC, Weekes CD, Jimeno A, Leong S, Pitts TM, et al. Patient-derived tumour xenografts as models for oncology drug development. Nat Rev Clin Oncol 2012;9:338–50.
21. Day CP, Merlino G, Van Dyke T. Preclinical mouse cancer models: a maze of opportunities and challenges. Cell 2015;163:39–53.
22. Daniel VC, Marchionni L, Hierman JS, Rhodes JT, Devereux WL, Rudin CM, et al. A primary xenograft model of small-cell lung cancer reveals irreversible changes in gene expression imposed by culture *in vitro*. Cancer Res 2009;69:3364–73.
23. Bertotti A, Migliardi G, Galimi F, Sassi F, Torti D, Isella C, et al. A molecularly annotated platform of patient-derived xenografts ("xenopatients") identifies HER2 as an effective therapeutic target in cetuximab-resistant colorectal cancer. Cancer Discov 2011;1:508–23.
24. Bertotti A, Papp E, Jones S, Adleff V, Anagnostou V, Lupo B, et al. The genomic landscape of response to EGFR blockade in colorectal cancer. Nature 2015;526:263–7.
25. DeRose YS, Wang G, Lin YC, Bernard PS, Buys SS, Ebbert MT, et al. Tumor grafts derived from women with breast cancer authentically reflect tumor pathology, growth, metastasis and disease outcomes. Nat Med 2011;17:1514–20.
26. Gao H, Korn JM, Ferretti S, Monahan JE, Wang Y, Singh M, et al. High-throughput screening using patient-derived tumor xenografts to predict clinical trial drug response. Nat Med 2015;21:1318–25.
27. Arrowsmith J.Trial watch: Phase II failures: 2008–2010. Nat Rev Drug Discov 2011;10:328–9.
28. Arrowsmith J, Miller P. Trial watch: phase II and phase III attrition rates 2011–2012. Nat Rev Drug Discov 2013;12:569.
29. Paul SM, Mytelka DS, Dunwiddie CT, Persinger CC, Munos BH, Lindborg SR, et al. How to improve R&D productivity: the pharmaceutical industry's grand challenge. Nat Rev Drug Discov 2010;9:203–14.
30. Cottu P, Bieche I, Assayag F, El Botty R, Chateau-Joubert S, Thuleau A, et al. Acquired resistance to endocrine treatments is associated with tumor-specific molecular changes in patient-derived luminal breast cancer xenografts. Clin Cancer Res 2014;20:4314–25.
31. Ter Brugge P, Kristel P, van der Burg E, Boon U, de Maaker M, Lips E, et al. Mechanisms of therapy resistance in patient-derived xenograft models of BRCA1-deficient breast cancer. J Natl Cancer Inst 2016;108:1–12.
32. Rubio-Viqueira B, Jimeno A, Cusatis G, Zhang X, Iacobuzio-Donahue C, Karikari C, et al. An *in vivo* platform for translational drug development in pancreatic cancer. Clin Cancer Res 2006;12:4652–61.
33. Damhofer H, Ebbing EA, Steins A, Welling L, Tol JA, Krishnadath KK, et al. Establishment of patient-derived xenograft models and cell lines for malignancies of the upper gastrointestinal tract. J Transl Med 2015;13:115.
34. Kwak EL, Bang YJ, Camidge DR, Shaw AT, Solomon B, Maki RG, et al. Anaplastic lymphoma kinase inhibition in non-small-cell lung cancer. N Engl J Med 2010;363:1693–703.
35. Roth A, Ding J, Morin R, Crisan A, Ha G, Giuliany R, et al. JointSNVMix: a probabilistic model for accurate detection of somatic mutations in normal/tumour paired next-generation sequencing data. Bioinformatics 2012;28:907–13.
36. Larson DE, Harris CC, Chen K, Koboldt DC, Abbott TE, Dooling DJ, et al. SomaticSniper: identification of somatic point mutations in whole genome sequencing data. Bioinformatics 2012;28:311–7.
37. Koboldt DC, Zhang Q, Larson DE, Shen D, McLellan MD, Lin L, et al. VarScan 2: somatic mutation and copy number alteration discovery in cancer by exome sequencing. Genome Res 2012;22:568–76.
38. Sherry ST, Ward MH, Kholodov M, Baker J, Phan L, Smigielski EM, et al. dbSNP: the NCBI database of genetic variation. Nucleic Acids Res 2001;29:308–11.
39. Auton A, Brooks LD, Durbin RM, Garrison EP, Kang HM, Korbel JO, et al. A global reference for human genetic variation. Nature 2015;526:68–74.
40. Lek M, Karczewski KJ, Minikel EV, Samocha KE, Banks E, Fennell T, et al. Analysis of protein-coding genetic variation in 60,706 humans. Nature 2016;536:285–91.
41. Forbes SA, Beare D, Boutselakis H, Bamford S, Bindal N, Tate J, et al. COSMIC: somatic cancer genetics at high-resolution. Nucleic Acids Res 2017;45:D777–83.
42. Ng PC, Henikoff S. SIFT: Predicting amino acid changes that affect protein function. Nucleic Acids Res 2003;31:3812–4.
43. Adzhubei I, Jordan DM, Sunyaev SR. Predicting functional effect of human missense mutations using PolyPhen-2. Curr Protoc Hum Genet 2013;7:Unit7 20.
44. Cingolani P, Platts A, Wang le L, Coon M, Nguyen T, Wang L, et al. A program for annotating and predicting the effects of single nucleotide polymorphisms, SnpEff: SNPs in the genome of *Drosophila melanogaster* strain w1118; iso-2; iso-3. Fly 2012;6:80–92.
45. Wang YC, Zuraek MB, Kosaka Y, Ota Y, German MS, Deneris ES, et al. The ETS oncogene family transcription factor FEV identifies serotonin-producing cells in normal and neoplastic small intestine. Endocr Relat Cancer 2010;17:283–91.
46. Wang YC, Gallego-Arteche E, Iezza G, Yuan X, Matli MR, Choo SP, et al. Homeodomain transcription factor NKX2.2 functions in immature cells to control enteroendocrine differentiation and is expressed in gastrointestinal neuroendocrine tumors. Endocr Relat Cancer 2009;16:267–79.
47. Reubi JC, Waser B. Concomitant expression of several peptide receptors in neuroendocrine tumours: molecular basis for *in vivo* multireceptor tumour targeting. Eur J Nucl Med Mol Imaging 2003;30:781–93.
48. Mojtahedi A, Thamake S, Tworowska I, Ranganathan D, Delpassand ES. The value of (68)Ga-DOTATATE PET/CT in diagnosis and management of neuroendocrine tumors compared to current FDA approved imaging modalities: a review of literature. Am J Nucl Med Mol Imaging 2014;4:426–34.
49. Hyman DM, Taylor BS, Baselga J. Implementing genome-driven oncology. Cell 2017;168:584–99.
50. Waddell N, Pajic M, Patch AM, Chang DK, Kassahn KS, Bailey P, et al. Whole genomes redefine the mutational landscape of pancreatic cancer. Nature 2015;518:495–501.
51. Song MS, Salmena L, Pandolfi PP. The functions and regulation of the PTEN tumour suppressor. Nat Rev Mol Cell Biol 2012;13:283–96.
52. Meric-Bernstam F, Akcakanat A, Chen H, Do KA, Sangai T, Adkins F, et al. PIK3CA/PTEN mutations and Akt activation as markers of sensitivity to allosteric mTOR inhibitors. Clin Cancer Res 2012;18:1777–89.
53. Yao JC, Phan AT, Jehl V, Shah G, Meric-Bernstam F. Everolimus in advanced pancreatic neuroendocrine tumors: the clinical experience. Cancer Res 2013;73:1449–53.
54. Thakker RV.Multiple endocrine neoplasia type 1 (MEN1). Best Pract Res Clin Endocrinol Metab 2010;24:355–70.
55. Chamberlain CE, Scheel DW, McGlynn K, Kim H, Miyatsuka T, Wang J, et al. Menin determines K-RAS proliferative outputs in endocrine cells. J Clin Invest 2014;124:4093–101.
56. Sadanandam A, Wullschleger S, Lyssiotis CA, Grotzinger C, Barbi S, Bersani S, et al. A cross-species analysis in pancreatic neuroendocrine tumors reveals molecular subtypes with distinctive clinical, metastatic, developmental, and metabolic characteristics. Cancer Discov 2015;5:1296–313.
57. Bryant HE, Schultz N, Thomas HD, Parker KM, Flower D, Lopez E, et al. Specific killing of BRCA2-deficient tumours with inhibitors of poly(ADP-ribose) polymerase. Nature 2005;434:913–7.
58. Mateo J, Carreira S, Sandhu S, Miranda S, Mossop H, Perez-Lopez R, et al. DNA-repair defects and olaparib in metastatic prostate cancer. N Engl J Med 2015;373:1697–708.